Journal of Solid State Chemistry **168,** 524–534 (2002)
doi:10.1006/jssc.2002.9750

Trifluoromethylsulfonyl-Based Salts of BEDT-TTF: Crystal and Electronic Structures and Physical Properties[1]

John A. Schlueter,*,[2] Urs Geiser,* H. Hau Wang,* Aravinda M. Kini,* Brian H. Ward,* James P. Parakka,* Roxanne G. Daugherty,* Margaret E. Kelly,* Paul G. Nixon,† Rolf W. Winter,† Gary L. Gard,† Lawrence K. Montgomery,‡ H.-J. Koo,§ and M.-H. Whangbo§

*Materials Science Division, Argonne National Laboratory, 9700 South Cass Ave., Bldg. 200, Argonne, IL 60439-4831; †Department of Chemistry, Portland State University, Portland, OR 97207-0751; ‡Department of Chemistry, Indiana University, Bloomington, IN 47405, USA; and §Department of Chemistry, North Carolina State University, Raleigh, NC 27695-8204

Received January 8, 2002; in revised form April 5, 2002; accepted April 11, 2002

Three 2 : 1 salts of the organic donor molecule bis(ethylenedithio)tetrathiafulvalene (BEDT-TTF or ET) with trifluoromethylsulfonyl-based anions $N(SO_2CF_3)_2^-$, $CH(SO_2CF_3)_2^-$ and $C(SO_2CF_3)_3^-$ were prepared by electrocrystallization. These salts were characterized by single-crystal X-ray diffraction, electron spin resonance (ESR) spectroscopy, electrical resistivity measurements and electronic band structure calculations. $(ET)_2N(SO_2CF_3)_2$ is a two-dimensional (2D) metal, but its ESR spin susceptibility above 150 K shows a weakly semiconducting behavior, presumably because during ESR measurements the sample cooling rate is slow hence allowing the disordered anions to readjust their positions. $(ET)_2CH(SO_2CF_3)_2$ is a 2D metal and undergoes a metal-to-insulator (MI) transition at 110 K due probably to a geometry change of the donor molecule layers. $(ET)_2C(SO_2CF_3)_3$ is a one-dimensional (1D) metal and undergoes an MI between 180 and 240 K, which is expected to be of charge density wave type. © 2002 Elsevier Science (USA)

Key Words: **BEDT-TTF; trifluoromethylsulfonyl anions; charge transfer salt; electrical conductivity.**

1. INTRODUCTION

Over the past two decades a number of new organic superconductors and charge transfer salts with novel electrical and magnetic properties have been prepared (1–4) using the donor molecule, bis(ethylenedithio) tetrathiafulvalene (BEDT-TTF or ET). In fact, well over half the organic radical cation-based superconductors are derived from ET, including κ-$(ET)_2Cu[N(CN)_2]Cl$ with the highest superconducting transition temperature T_c (12.5 K under 0.3 kbar pressure) (5), which consists of polymeric $Cu[N(CN)_2]Cl^-$ anions. We have demonstrated that large discrete fluorinated anions, $M(CF_3)_4^-$ (M = Cu, Ag, Au), lead to two families of superconducting salts (6). Fifteen solvated salts of the type, κ_L-$(ET)_2M(CF_3)_4$(1,1,2-trihaloethane), have T_c values in the 2–6 K range (7–11). Six related salts of the same stoichiometry, κ_H-$(ET)_2M(CF_3)_4$(1,1,2-trihaloethane), have T_c values in the 7–11 K range. In contrast, the non-solvated salts, $(ET)_2M(CF_3)_4$, are semiconductors (12). More recently, we discovered superconductivity in an ET salt of the highly fluorinated $SF_5CH_2CF_2SO_3^-$ anion, β''-$(ET)_2SF_5CH_2CF_2SO_3$ ($T_c = 4.4$ K) [13].

Highly fluorinated anions have thus been shown to be promising components of molecular superconductors. This may be due in part to the interlayer coupling resulting from hydrogen-bonding H···F contacts between the electronegative fluorine atoms in the anion layer and the hydrogen atoms of ET, which are located on the periphery of the donor layer. In order to more fully address the relevance of these interlayer hydrogen-bonding contacts, we have sought to prepare charge transfer salts of ET that contain similar, fluorinated monovalent anions. The physical properties of ET salts can change dramatically when their structures are altered by a slight chemical modification of their charge compensating anions.

Lithium bis(trifluoromethanesulfonyl)imide, $LiN(SO_2CF_3)_2$, and lithium tris(trifluoromethanesulfonyl)-methide, $LiC(SO_2CF_3)_3$, were developed as components

[1]Work at Argonne National Laboratory is sponsored by the US Department of Energy, Office of Basic Energy Sciences, Division of Materials Sciences. The submitted manuscript has been authored by a contractor of the US Government under Contract W-31-109-ENG-38. Accordingly, the US Government retains a non-exclusive, royalty-free license to publish or reproduce the published form of this contribution, or allow others to do so for US Government purposes.

[2]To whom correspondence should be addressed. Tel.: + 1-630-252-3588; Fax: + 1-630-252-9151. E-mail: jaschlueter@anl.gov.

0022-4596/02 $35.00

for organic electrolyte-based lithium batteries (14). These compounds have excellent electrochemical and thermal stability in part because their negative charge is delocalized into the electron-withdrawing groups CF_3 and SO_2 (14). More recently, similar physical properties were observed for the more easily prepared lithium bis(trifluoromethanesulfonyl)methide, $LiCH(SO_2CF_3)_2$ (15). The three anions, $N(SO_2CF_3)_2^-$, $CH(SO_2CF_3)_2^-$, and $C(SO_2CF_3)_3^-$, of these lithium salts possess many similarities: charge distribution, size, peripheral trifluoromethanesulfonate groups, etc. Our electrocrystallization of ET with these anions produced a number of ET salts, e.g., $(ET)_2N(SO_2CF_3)_2$, $(ET)_2CH(SO_2CF_3)_2$, $(ET)_2C(SO_2CF_3)_3$ and $(ET)C(SO_2CF_3)_3$. In the present work, we compare the crystal structures, physical properties and electronic structures of the three 2 : 1 salts: $(ET)_2N(SO_2CF_3)_2$, $(ET)_2CH(SO_2CF_3)_2$ and $(ET)_2C(SO_2CF_3)_3$. Preliminary results on the crystal structure and Raman and ESR properties of $(ET)_2N(SO_2CF_3)_2$ were reported earlier (16).

2. EXPERIMENTAL

2.1. Synthesis

ET was prepared as previously described (17, 18) and recrystallized from chloroform (Aldrich) prior to use. $LiC(SO_2CF_3)_3$ (Covalent Associates, Inc., Woburn, MA, USA), 12-crown-4 (Aldrich) and $LiN(SO_2CF_3)_2$ (3 M, St. Paul, MN, USA), were used as received. $LiCH(SO_2CF_3)_2$ was prepared as previously described (15). 1,1,2-Trichloroethane (TCE, Fluka) was distilled from P_2O_5 (Aldrich) and filtered through a column containing neutral alumina prior to use. Tetrahydrofuran (THF) was distilled from sodium/benzophenone prior to use. Dichloromethane (Aldrich, 99.9%, A.C.S. HPLC grade) and chlorobenzene (Aldrich, 99.6%, A.C.S. reagent) were used without further purification. Elemental analyses were performed at Galbraith Laboratories (Knoxville, TN, USA) and Midwest Microlab (Indianapolis, IN, USA).

Black rod-like crystals of $(ET)_2C(SO_2CF_3)_3$ were grown by using the previously described electrocrystallization techniques (19, 20). The electrochemical cell was assembled in a dry box filled with argon. Excess $LiC(SO_2CF_3)_3$ and three drops of 12-crown-4 were added to both chambers of an H-cell. ET (7.90 mg, 0.021 mmol) was loaded into the anode chamber. The crystallization solvent, chlorobenzene (7.5 mL), was then added to each chamber. A current density of 0.19 $\mu A/cm^2$ was initially applied and gradually increased over a period of 6 days to 1.21 $\mu A/cm^2$, at which time crystallization of black crystals commenced. Crystals were grown at 25°C on platinum wire electrodes for a period of 12 days. Rod-like crystals of $(ET)_2C(SO_2CF_3)_3$ as well as block-like crystals of the 1:1 salt $(ET)C(SO_2CF_3)_3$ [21] grew side by side in the same electrocrystallization cells. The best $(ET)_2C(SO_2CF_3)_3$ crystals grew when dichloromethane was used as the solvent. Similar electrocrystallization procedures with THF as the solvent produced small block-like crystals of $(ET)C(SO_2CF_3)_3$, while use of 1,1,2-trichloroethane as solvent resulted in a greater percentage of black rod-like crystals.

Black block-like crystals of $(ET)_2CH(SO_2CF_3)_2$ were grown as described above, except that $LiCH(SO_2CF_3)_2$ replaced $LiC(SO_2CF_3)_3$ as the supporting electrolyte. The best crystals were grown with the use of TCE as crystallization solvent. Crystallization occurred on the floor of the anode chamber, rather than on the anode surface. Crystallization commenced after 7 days, and was continued for a total of 34 days. Only one crystalline phase of $(ET)_2CH(SO_2CF_3)_2$ was observed by ESR line width characterization (11–15 G). Poorer quality crystals resulted when THF was used as the crystallization solvent, and no crystal growth occurred when benzonitrile was used.

Black block- and rod-like crystals of $(ET)_2N(SO_2CF_3)_2$ were grown as previously reported [16] by using $LiN(SO_2CF_3)_2$ as the supporting electrolyte. Good-quality crystals were grown using either THF, TCE or chlorobenzene as the crystallization solvent and current densities between 0.2 and 0.8 $\mu A/cm^2$. Under these growth conditions, only one crystalline phase was observed by ESR line width characterization (28–38 G). Crystals of $(ET)_2N(SO_2CF_3)_2$ could also be grown using $(PPN)N(SO_2CF_3)_2$ [PPN = bis(triphenylphosphoranylidene)ammonium] as the supporting electrolyte with TCE as the crystallization solvent. With this electrolyte, a second crystalline phase also grew, which has a much narrower line width of 7 G. Characterization of this phase is in progress.

2.2. Physical Measurements

Electron spin resonance (ESR) measurements were performed on an IBM ER-200 X-band spectrometer equipped with a TE_{102} microwave cavity and an Oxford EPR-900 flow cryostat with an ITC4 temperature controller. The single-crystal structures of $(ET)_2N(SO_2CF_3)_2$, $(ET)_2CH(SO_2CF_3)_2$ and $(ET)_2C(SO_2CF_3)_3$ were determined at 296 K by X-ray diffraction using a Siemens SMART® single crystal X-ray diffractometer equipped with a CCD-based area detector and a sealed-tube X-ray source. Further details are deposited as Supporting Information. The temperature dependence of the electrical resistivity was measured by using the conventional four-probe technique with a LakeShore Model 7000 cryostat equipped with RES7000 software. The current and voltage contacts were made with a gold wire (0.0005 in diameter) attached to the crystal with silver conducting paste. Resistivity data were recorded during both the cooling and warming cycles, and a slow cooling/warming rate of

about 1°/min was utilized to prevent microcracking of either the crystal or contacts. A DC current of 0.5 mA was applied.

3. CRYSTAL STRUCTURES

In $(ET)_2N(SO_2CF_3)_2$, $(ET)_2CH(SO_2CF_3)_2$ and $(ET)_2C(SO_2CF_3)_3$, the layers of the ET molecules are separated by the anion layers, as depicted in Figs. 1a–1c, respectively. Figure 2 shows the atom numbering used for the donor molecules of all three salts, and Fig. 3 that used for the $N(SO_2CF_3)_2^-$, $CH(SO_2CF_3)_2^-$ and $C(SO_2CF_3)_3^-$ anions. Table 1 summarizes the crystallographic data for these ET salts.

The $(ET)_2N(SO_2CF_3)_2$ salt has one donor layer per unit cell, in which all ET molecules are equivalent. The ethylene end groups of the ET electron-donor molecules are ordered in an eclipsed manner. The donor stacks are arranged such that ET molecules in different stacks form nearly coplanar arrays along the interstack direction (Fig. 4a), as found for the β''-type salts (22), such as β''-$(ET)_2SF_5CH_2SO_3$ and β''-$(ET)_2SF_5CHFSO_3$ (23). All intermolecular S…S contacts shorter than the sum of the van der Waals radii (3.60 Å) are located in ribbons along the *a*-axis. According to the empirical correlation between the central C–S/C=C bond lengths of ET and the partial oxidation state of ET in ET salts (24), the oxidation state of the ET molecules in $(ET)_2N(SO_2CF_3)_2$ is estimated to be +0.59, which is not far from +0.50 required by the stoichiometry of the compound.

The $N(SO_2CF_3)_2^-$ anion in $(ET)_2N(SO_2CF_3)_2$ is disordered about two positions related by an inversion center (16). In this salt, the anion adopts a *transoid* configuration, in which the CF_3 groups are located on opposite sides of the plane defined by the S–N–S bonds. This is in contrast to the cisoid conformation observed in $KN(SO_2CF_3)_2$ (25), but similar to the *transoid* structure determined for $LiN(SO_2CF_3)_2$ [26], $[Mg(H_2O)_6][N(SO_2CF_3)_2]_2 \cdot H_2O$ (27), and the salt containing the very weakly interacting 1-ethyl-2-methyl-3-benzyl imidazolium cation (28). The $N(SO_2CF_3)_2^-$ anion in $(ET)_2N(SO_2CF_3)_2$ has an S–N–S bond angle of 121.1(5)°, which is slightly more acute than those previously reported for this anion (125–129°) (25–28). The S–N bond length of 1.573(10) Å, is typical for the $N(SO_2CF_3)_2^-$ anion (25–28), but 0.07 Å shorter than that observed in $HN(SO_2CF_3)_2$ (25).

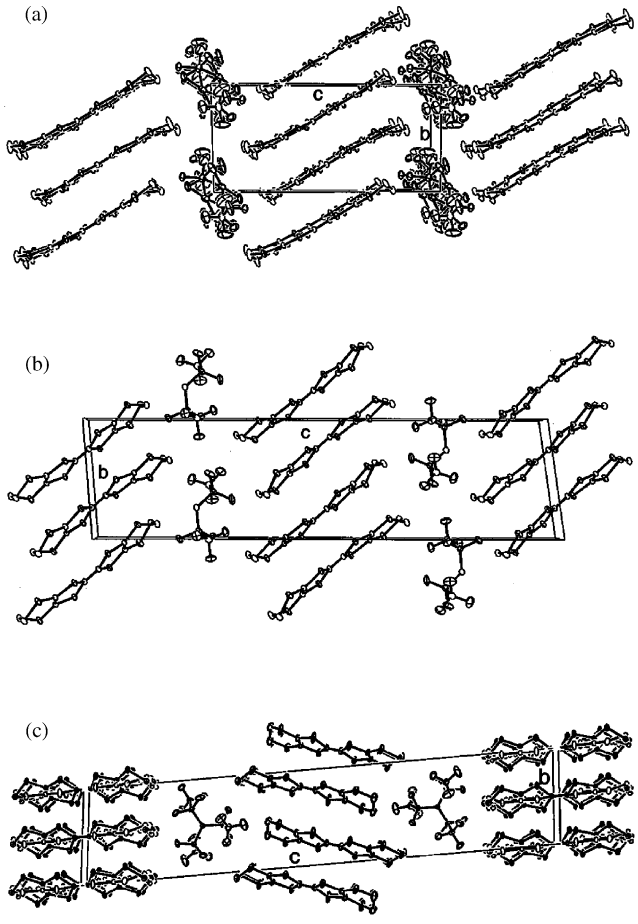

FIG. 1. Perspective views of the donor and anion layers in (a) $(ET)_2N(SO_2CF_3)_2$, (b) $(ET)_2CH(SO_2CF_3)_2$ and (c) $(ET)_2C(SO_2CF_3)_3$.

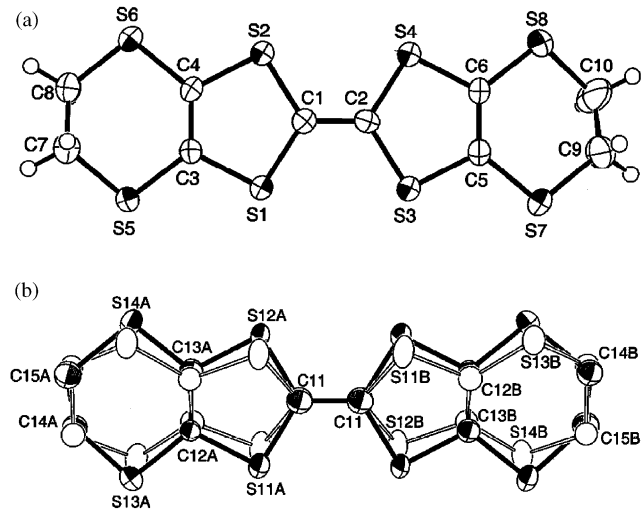

FIG. 2. Numbering scheme of the atoms of the ET electron-donor molecules. Scheme (a) is used for $(ET)_2N(SO_2CF_3)_2$, and one of the crystallographically unique ET molecules of the $(ET)_2CH(SO_2CF_3)_2$ and $(ET)_2C(SO_2CF_3)_3$ structures. The numbering of the second crystallographically unique molecule of the $(ET)_2CH(SO_2CF_3)_2$ structure is obtained by adding 10 to each of the atom labels. The numbering of the second crystallographically unique ET molecule of the $(ET)_2C(SO_2CF_3)_3$ salt is shown in (b). The unshaded atoms depict the second possible orientation of the ET molecule. By adding 10 to these atom labels, the numbering scheme of the third unique ET molecule of the $(ET)_2C(SO_2CF_3)_3$ structure is obtained. The hydrogen atoms of the ET molecule have been omitted in (b) for clarity.

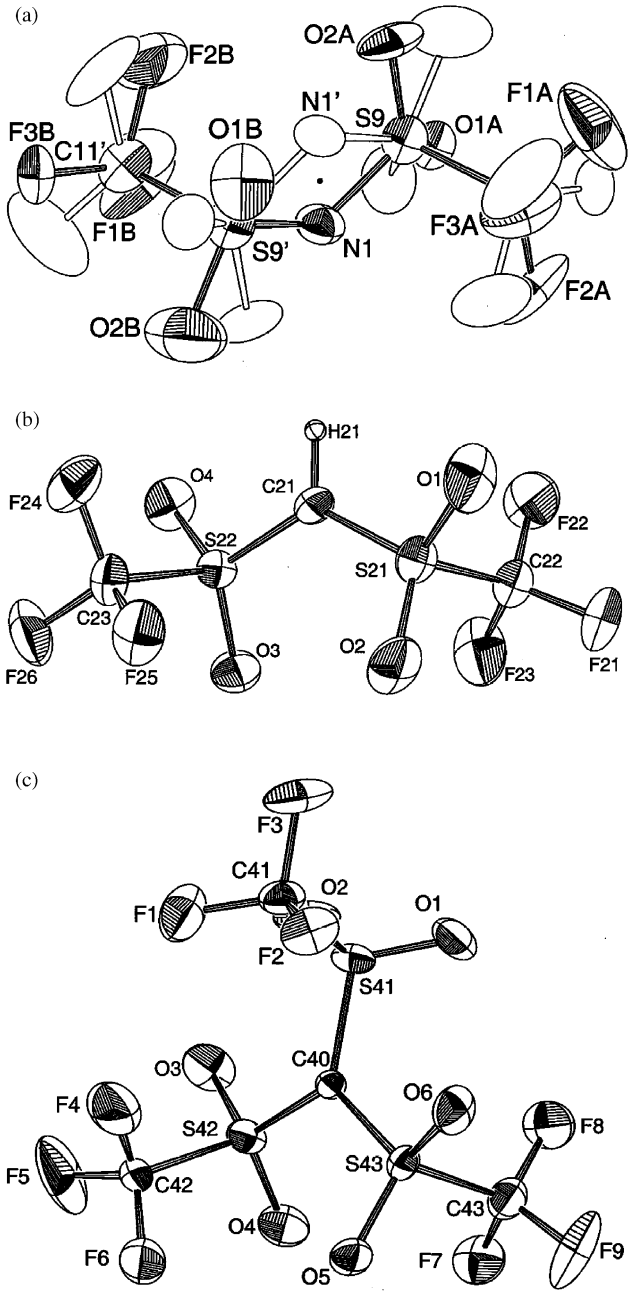

FIG. 3. Numbering of the atoms of the anions employed for (a) $(ET)_2N(SO_2CF_3)_2$, (b) $(ET)_2CH(SO_2CF_3)_2$ and (c) $(ET)_2C(SO_2CF_3)_3$.

The $(ET)_2CH(SO_2CF_3)_2$ salt is an ordered superstructure of the $(ET)_2N(SO_2CF_3)_2$ structure. It contains two crystallographically non-equivalent donor layers per unit cell. Within each donor layer, all ET molecules are identical. The ethylene end groups of the ET molecules in both donor layers are ordered in an eclipsed conformation. Figures 4b and c show the arrangements of the ET molecules in the two non-equivalent donor layers of $(ET)_2CH(SO_2CF_3)_2$. The two layers have a very similar β-type packing motif (22). Based on the central C=C and C–S bond lengths, the ET molecules in Layer 1 ($z = 0.5$) are estimated to have a charge of $+0.56$, and those in Layer 2 ($z = 0$) have a charge of $+0.42$. The sum of these charges agrees well with the stoichiometry of the salt.

The $CH(SO_2CF_3)_2^-$ anion in the $(ET)_2CH(SO_2CF_3)_2$ salt is ordered in a transoid conformation. The transoid and cisoid conformations of the $CH(SO_2CF_3)_2^-$ anion have very similar energies: the transoid structure is observed in the p-$CH_3C_6H_4N_2^+$ (29) and trans-$(Ph_3P)_2Pt(H_2O)(PhC{=}CHPh)^+$ (30) salts while the cisoid conformation has been observed in the Rb^+, Cs^+ (31) and $(Ph_3P)_4OsH_3^+$ (32) salts. The S–C–S angle of 125.3(3)° in the $CH(SO_2CF_3)_2^-$ anion of $(ET)_2CH(SO_2CF_3)_2$ is typical of that previously reported (123–126.3° (29–32). Similarly, the central C–S bond lengths, 1.636(5) Å and 1.671(4) Å, are typical for this anion (1.65–1.68 Å) (29–32). The vertex of the S–C–S angle points toward ET Layer 1, whereas the ethylene end groups of ET Layer 2 are exposed primarily to the CF_3 end groups of the anion. This accounts for the difference in oxidation states observed for the two layers.

The ET layers of the $(ET)_2C(SO_2CF_3)_3$ salt also has two crystallographically non-equivalent donor layers per unit cell. In contrast to $(ET)_2CH(SO_2CF_3)_2$, the two non-equivalent donor layers of $(ET)_2C(SO_2CF_3)_3$ have significantly different packing motifs, as shown in Figs. 4d and 4e. The layer centered at $z = 0.5$ (Layer 1) consists of identical ET molecules with staggered ethylene end groups and packs in a β' structural motif (Fig. 4d). Figure 5a shows two possible arrangements of ET molecules that exist in the layer located at $z = 0$ (Layer 2). The S···S contacts shown in Fig. 5a are unphysically short: between 2.85 and 3.30 Å. Within a stack, these short contacts would exist only if molecules of A and B configurations are adjacent. Thus, within a stack, all molecules must be of either A or B configuration. Similarly, unphysically short intrastack contacts are observed if molecules of adjacent stacks have the same configuration (A or B). Thus, stacks of configuration A must alternate with stacks of configuration B, as shown in Figs. 4e and 5b. In each donor stack there are two different ET molecules, as indicated by labels 1 and 2 in Fig. 5b. The observation of diffuse rows of intensity at half-integer Miller index h in the diffraction pattern supports this interpretation of the disorder model. The packing within this layer is θ-type (33). Because these layers are separated by more than 40 Å, the packing in one layer is not influenced by that in an adjacent layer. Thus, if the layer located at $z = 0$ packs ABAB, the layer located at $z = 1$ can pack either ABAB or BABA with essentially no preference of one over the other.

The empirical relationship that relates the central C–S and C=C bond lengths of ET to the partial oxidation state of ET [24] is reliable only when the crystal structures of ET salts are accurate. We did not perform this analysis for

TABLE 1
Summary of Crystallographic Data for Three ET Salts That Contain Trifluoromethylsulfonyl-Based Anions

	$(ET)_2N(SO_2CF_3)_2$	$(ET)_2CH(SO_2CF_3)_2$	$(ET)_2C(SO_2CF_3)_3$
Chemical formula	$(C_{10}H_0S_8)_2N(SO_2CF_3)_2$	$(C_{10}H_0S_8)_2CH(SO_2CF_3)_2$	$(C_{10}H_0S_8)_2C(SO_2CF_3)_3$
Formula weight ($g\,mol^{-1}$)	1049.56	1048.46	1180.51
a (Å)	6.6394(13)	6.5955(4)	6.2692(4)
b (Å)	8.658(2)	9.1370(5)	8.4218(6)
c (Å)	17.349(4)	33.038(2)	40.249(3)
α (deg)	85.30(2)	83.718(1)	94.566(1)
β (deg)	82.79(2)	89.005(1)	90.949(1)
γ (deg)	68.95(2)	69.734(1)	106.734(1)
V (Å^3)	922.7(4)	1856.1(2)	2026.9(2)
Z	1	2	2
Space group	$P\bar{1}$	$P\bar{1}$	$P\bar{1}$
Temperature (K)	295	295	298
λ (Å)	0.71073	0.71073	0.71073
ρ_{calcd}, ($g\,cm^{-3}$)	1.889	1.876	1.934
μ, (cm^{-1})	1.07	1.11	1.049
$R(F_o)^a$	0.057	0.057	0.082
$R_w(F_o)$	0.050	0.064	0.100

$^a R(F_o) = \sum ||F_o| - |F_c|| / \sum |F_o|,\ R_w(F_o) = \left[\sum w(|F_o| - |F_c|)^2 / \sum wF_o^2\right]^{1/2}$

$(ET)_2C(SO_2CF_3)_3$ because its crystal structure is not accurate enough (see Table 1).

The $C(SO_2CF_3)_3^-$ anions in the $(ET)_2C(SO_2CF_3)_3$ salt are ordered. Similar to the $C(SO_2CF_3)_3^-$ anion in the structure of $KC(SO_2CF_3)_3 \cdot H_2O$ [34], the CS_3 skeleton is planar with two of the CF_3 groups below this plane and one above.

4. PHYSICAL PROPERTIES

4.1. ESR

The ESR line widths and spin susceptibilities of $(ET)_2N(SO_2CF_3)_2$, $(ET)_2CH(SO_2CF_3)_2$, and $(ET)_2C(SO_2CF_3)_3$ were measured over the temperature range 5–300 K, as summarized in Figs. 6a–c, respectively. The line width of $(ET)_2C(SO_2CF_3)_3$ is near 30 G at room temperature, as in the case of $(ET)_2N(SO_2CF_3)_2$, while a much sharper line width (10–12 G) is observed for $(ET)_2CH(SO_2CF_3)_2$ at room temperature.

The spin susceptibility of $(ET)_2N(SO_2CF_3)_2$ is relatively constant at room temperature, decreases slowly between $\sim$250 and $\sim$150 K, decreases very slowly below $\sim$150 K, and becomes nearly constant below $\sim$50 K, where the susceptibility is about 35% of the value at room temperature (Fig. 6a). The Arrhenius-type plot of $\ln[\chi(T)/\chi(2\,8\,0)]$ versus $1/T$ using the susceptibility data for the 280–to 150 K region indicates a very small activation energy, $E_a = 18.7$ meV (16), indicating weak semiconducting behavior. Below $\sim$150 K the spin susceptibility remains substantial and its temperature dependence is weak so that $(ET)_2N(SO_2CF_3)_2$ should be considered to be weakly metallic. This behavior is reminiscent of that observed in the metallic β''-$(ET)_2SF_5CH_2CF_2SO_3$ system, which superconducts below 4.5 K (35).

In general, a metallic salt exhibits an at most weakly temperature-dependent spin susceptibility, while a nonmagnetic semiconducting salt shows a strong decrease in spin susceptibility with decreasing temperature. The spin susceptibility of $(ET)_2CH(SO_2CF_3)_2$ is nearly constant above $\sim$110 K, decreases sharply between $\sim$110 and $\sim$50 K, and remains at a very small value below $\sim$50 K (Fig. 6b). Thus, the spin susceptibility data indicate that $(ET)_2CH(SO_2CF_3)_2$ is metallic above $\sim$110 K, below which it undergoes a metal-to-insulator (MI) transition. The MI transition temperature, $\sim$110 K, is rather high, and the spin susceptibility below $\sim$110 K is very small. Thus, the MI transition leads to a normal semiconducting state rather than to a magnetic insulating state. We speculate that the MI transition is caused by a geometry change in the donor lattice rather than by electron localization associated with electron–electron repulsion (36–38).

The spin susceptibility of $(ET)_2C(SO_2CF_3)_3$ is relatively constant above $\sim$240 K, decreases sharply between $\sim$240 and $\sim$180 K, remains nearly constant at a small value between $\sim$180 and $\sim$50 K, and increases sharply below 50 K (Fig. 6c). Although the spin susceptibility is nearly constant between $\sim$180 and $\sim$50 K, the value is small so that $(ET)_2C(SO_2CF_3)_3$ should be regarded as an insulator in this temperature region. Thus, based on the ESR data, $(ET)_2C(SO_2CF_3)_3$ is metallic above $\sim$240 K and undergoes an MI transition between 180 and 240 K. The sharp increase in the susceptibility below $\sim$50 K is due most likely to the occurrence of spin impurities. (See below for the discussion of their probable origin.)

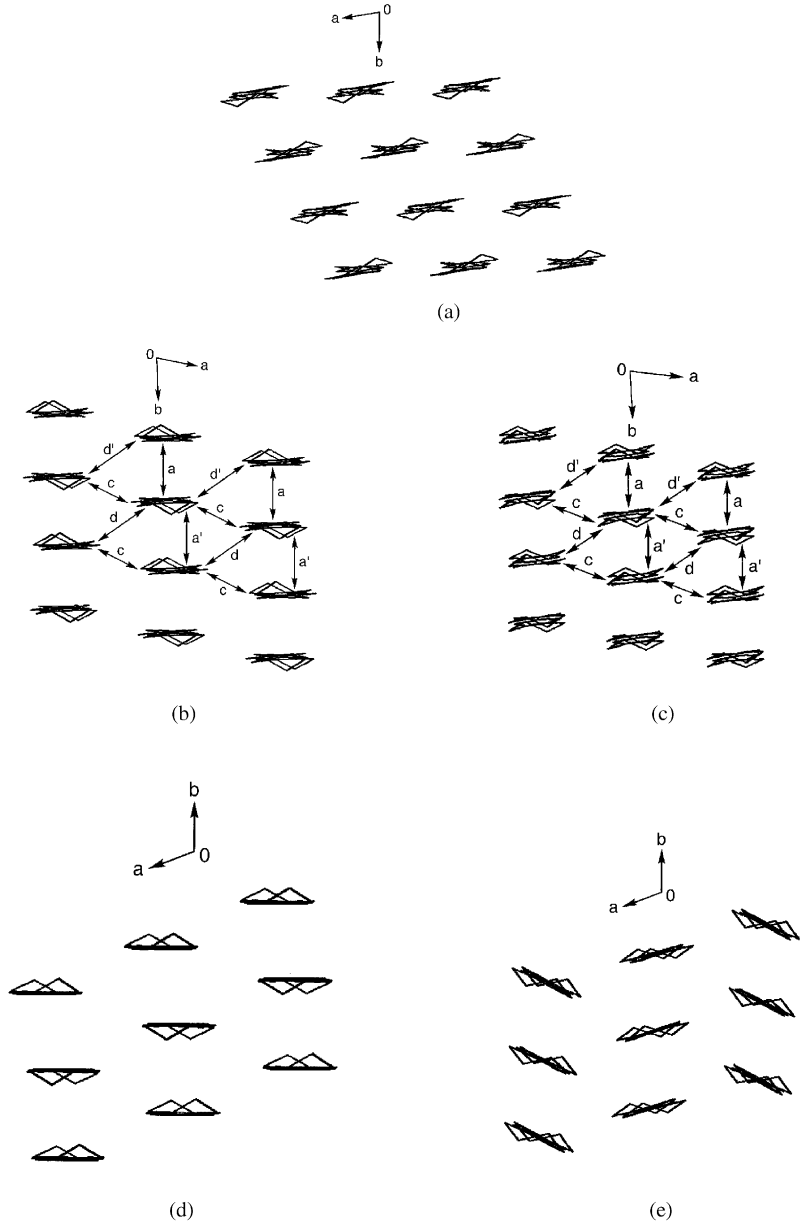

FIG. 4. Packing motifs of the ET molecules: (a) the donor layer of $(ET)_2N(SO_2CF_3)_2$, (b) the donor Layer 1 of $(ET)_2CH(SO_2CF_3)_2$, (c) the donor Layer 2 of $(ET)_2CH(SO_2CF_3)_2$, (d) the donor Layer 1 of $(ET)_2C(SO_2CF_3)_3$ and (e) the donor Layer 2 of $(ET)_2C(SO_2CF_3)_3$. In Fig. 4(e) one of the two disordered positions of ET was chosen. The labels between adjacent ET molecules define the nearest neighbors i and j for the HOMO–HOMO interaction energies β_{ij} listed in Table 2.

4.2. Resistivity

The electrical resistivities measured for single-crystal samples of $(ET)_2N(SO_2CF_3)_2$, $(ET)_2CH(CF_3SO_2)_2$, and $(ET)_2C(SO_2CF_3)_3$ are plotted as a function of temperature in Figs. 6a–c, respectively.

Figure 6a shows that $(ET)_2N(SO_2CF_3)_2$ is metallic over the whole temperature region studied, although the corresponding ESR spin susceptibility data indicate a weakly semiconducting behavior above ~ 150 K. This apparent discrepancy may originate from the difference in the rate of cooling the sample employed in the ESR and electrical resistivity measurements. A sample is kept at a given temperature for a much longer time during ESR measurements than during electrical resistivity measurements. Namely, the cooling rate is slower during ESR measurements. As pointed out already, the anion positions of $(ET)_2N(SO_2CF_3)_2$ are disordered so that at a given

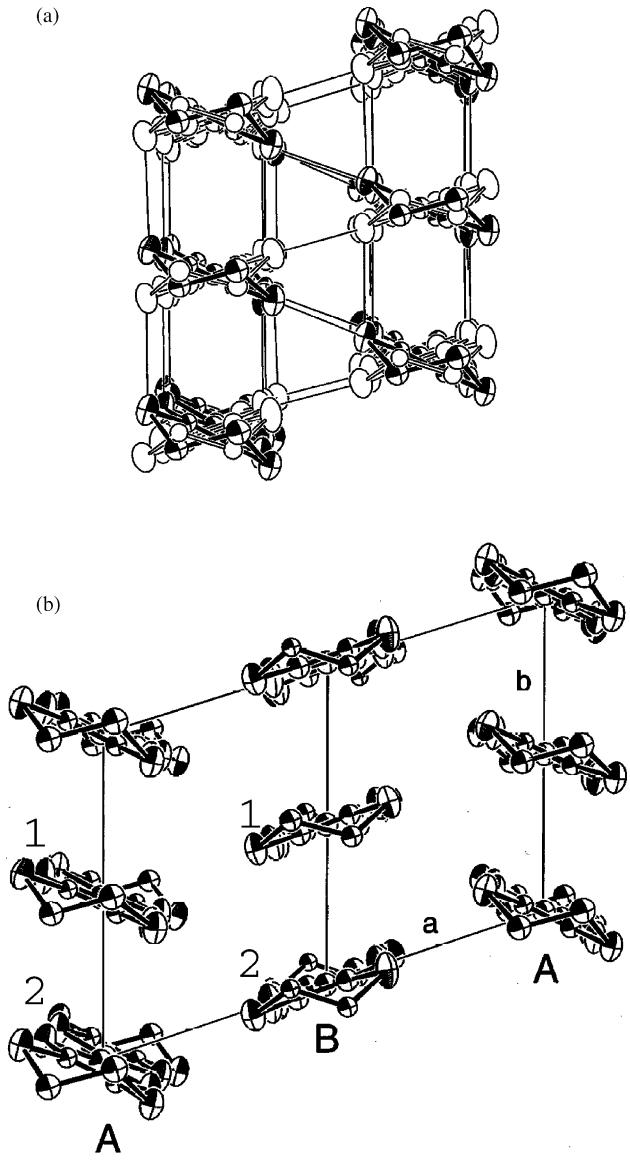

FIG. 5. Projection on the *ab*-plane of the donor layer of $(ET)_2C(SO_2CF_3)_3$ which contains two arrangements of ET molecules. (a) Superimposed are the two orientations of the ET molecules. Unphysically short S…S contacts, 2.85–3.3 Å are shown. (b) Within a single layer, there is no disorder. Adjacent stacks alternate between the A and B configurations to avoid steric interactions. The labels 1 and 2 in the donor stacks A and B are used to indicate the occurrence of two different ET molecules in each stack.

temperature the anions have more time to adjust their positions during ESR measurements. When the anions adjust their positions, the lattice phonon structures change and hence the mobility of electron carriers is modified. Then the weakly semiconducting behavior observed by ESR measurements implies that the mobility decreases as the temperature is lowered to ~ 150 K. This is reasonable for the following reasons: as the anion positions become frozen by lowering temperature, the extent of disorder should increase hence lowering the electron mobility. After all the anion positions are frozen at a certain temperature, a further temperature lowering cannot strongly influence the electron mobility. Thus, the ESR spin susceptibility of $(ET)_2N(SO_2CF_3)_2$ should exhibit a weak metallic character below a certain temperature. This is precisely what is found in Fig. 6a.

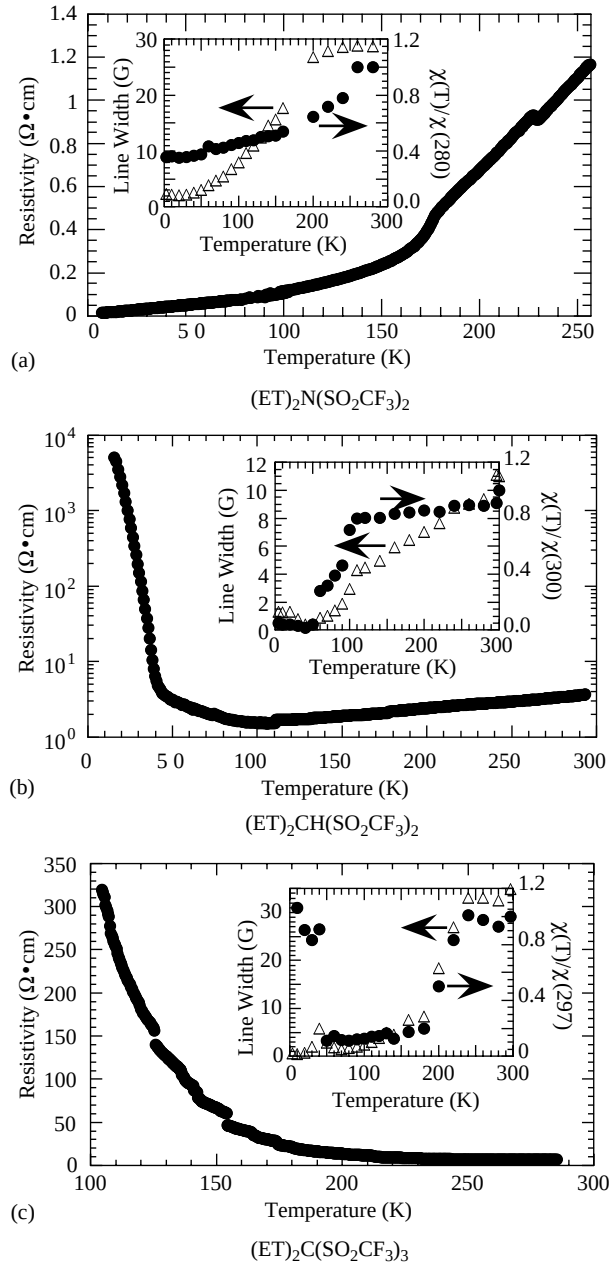

FIG. 6. Temperature dependence of the peak-to-peak line width, the spin susceptibility and conductivity of (a) $(ET)_2N(SO_2CF_3)_2$, (b) $(ET)_2CH(SO_2CF_3)_2$ and (c) $(ET)_2C(SO_2CF_3)_3$.

$(ET)_2CH(CF_3SO_2)_2$ has weakly metallic character down to $\sim$110 K, below which it shows a semiconducting behavior (Fig. 6b). These observations are consistent with the corresponding ESR spin susceptibility data. Fig. 6c reveals that the electrical resistivity of $(ET)_2C(SO_2CF_3)_3$ is non-metallic below $\sim$240 K and is practically temperature independent above $\sim$240 K. These findings are also consistent with the corresponding ESR spin susceptibility data.

5. ELECTRONIC STRUCTURES

Figure 7a shows the dispersion relations of the two HOMO bands (i.e., the highest two occupied bands derived largely from the HOMO's of ET molecules) calculated for $(ET)_2N(SO_2CF_3)_2$ using the extended Hückel tight binding method (39–41). The highest-lying band is half-filled, and the Fermi surface associated with this band is shown in Fig. 7b in an extended zone scheme. The Fermi surface is an ellipse centered at M. Thus $(ET)_2N(SO_2CF_3)_2$ is a two-dimensional (2D) metal. The predicted metallic character agrees with the result of the electrical resistivity measurements. The ellipses do not overlap, but nearly touch each other along the X → M line. Magnetoresistance experiments of this salt would be interesting, because it might undergo a magnetic breakdown under high magnetic field (42–44).

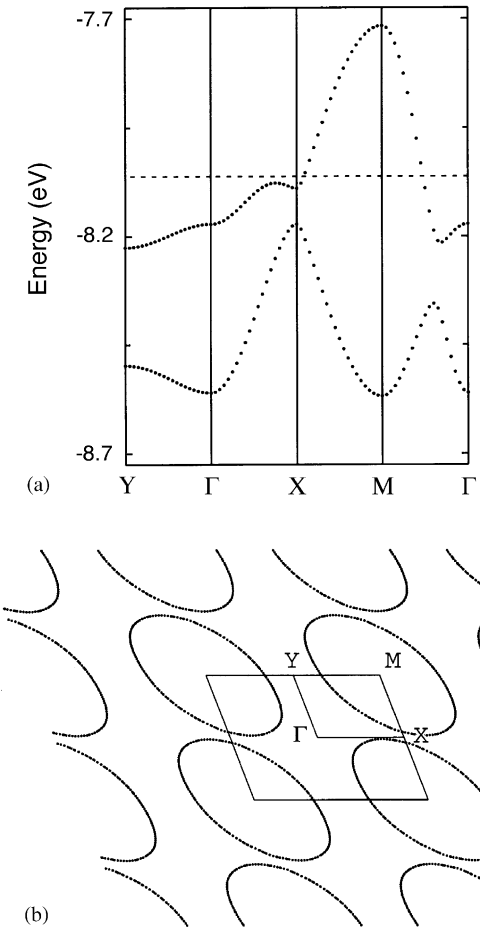

FIG. 7. (a) Dispersion relations of the two HOMO bands calculated for the donor layer of $(ET)_2N(SO_2CF_3)_2$. The dashed line refers to the Fermi level. (b) Fermi surface associated with the partially filled band of (a).

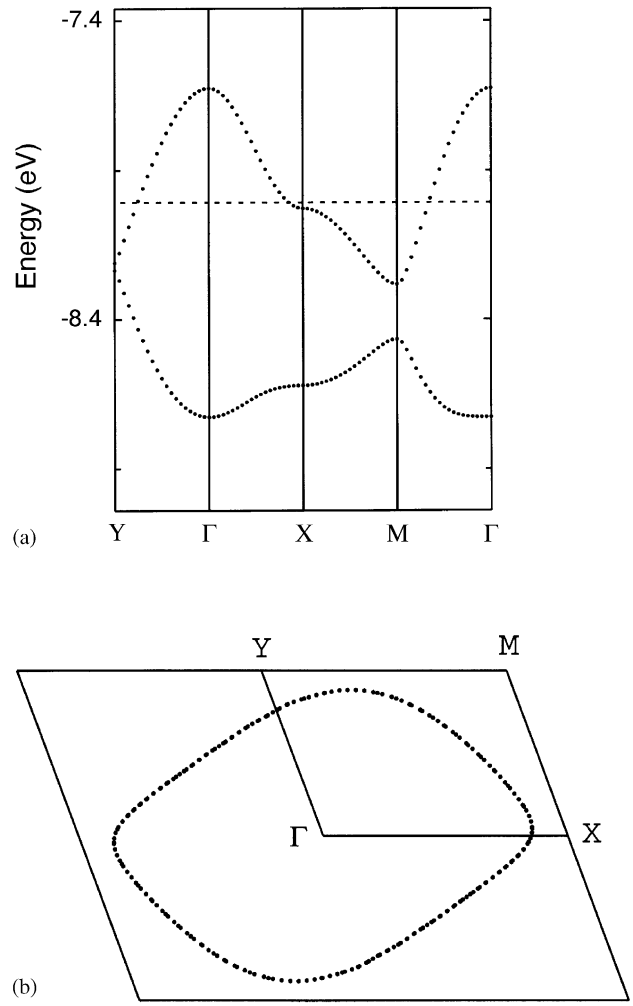

FIG. 8. (a) Dispersion relations of the two HOMO bands calculated for the donor Layer 1 of $(ET)_2CH(SO_2CF_3)_2$. The dashed line refers to the Fermi level. (b) Fermi surface associated with the partially filled band of (a).

Figure 8a shows the dispersion relations of the two HOMO bands calculated for donor Layer 1 of $(ET)_2CH(SO_2CF_3)_2$ (Fig. 4b). The highest-lying band is half-filled, and the Fermi surface associated with this band (Fig. 8b) is a distorted ellipse centered at Γ. Figures. 9a and b show the corresponding dispersion relations and the Fermi surface calculated for donor Layer 2 (Fig. 4c), respectively. Figures 8 and 9 show that Layers 1 and 2 are very similar, and $(ET)_2CH(SO_2CF_3)_2$ is a 2D metal. The predicted metallic

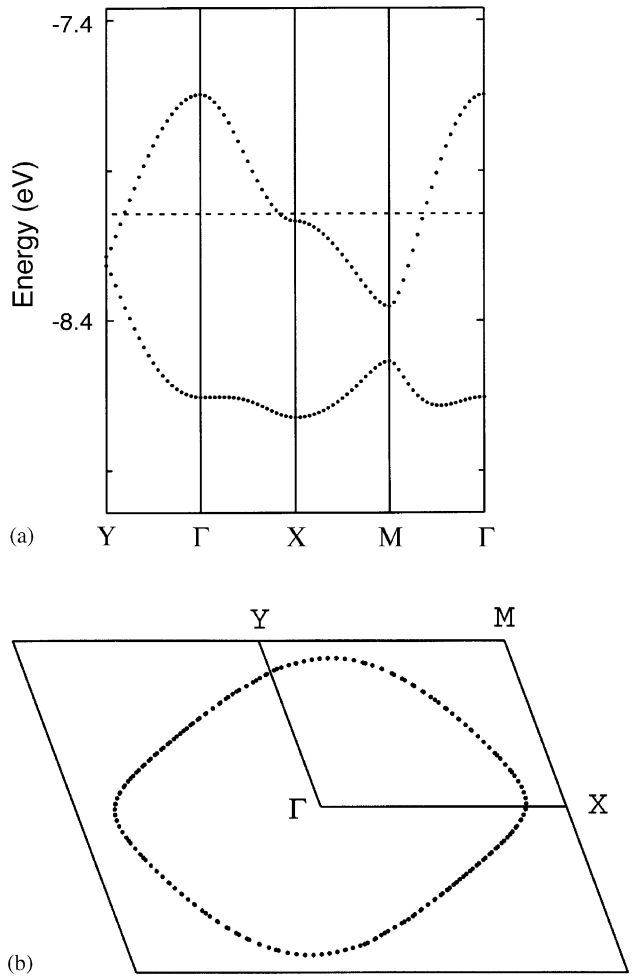

FIG. 9. (a) Dispersion relations of the two HOMO bands calculated for the donor Layer 2 of $(ET)_2CH(SO_2CF_3)_2$. The dashed line refers to the Fermi level. (b) Fermi surface associated with the partially filled band of (a).

property agrees with experiment for the temperature region above 110 K.

The crystal structure of $(ET)_2C(SO_2CF_3)_3$ is not so accurate, as already pointed out, so we consider only band dispersion relations in discussing the electronic structures of Layers 1 and 2 of $(ET)_2C(SO_2CF_3)_3$. Figure 10a shows the dispersion relations calculated for the two HOMO bands of Layer 1, and Fig. 10b those calculated for the four HOMO bands of Layer 2. Note that a unit cell has two ET molecules in Layer 1, but four in Layer 2. In essence, Layer 1 has a nearly half-filled band (Fig. 10a) while Layer 2 has a nearly empty band (Fig. 10b). The partial vacancy of the lower-lying band of Layer 1 around Y (Fig. 10a) is insignificant, and so is the partial occupancy of the highest-lying band of Layer 2 around X (Fig. 10b). This suggests that in average the oxidation state of ET is approximately +0.5 in both layers. The low accuracy of

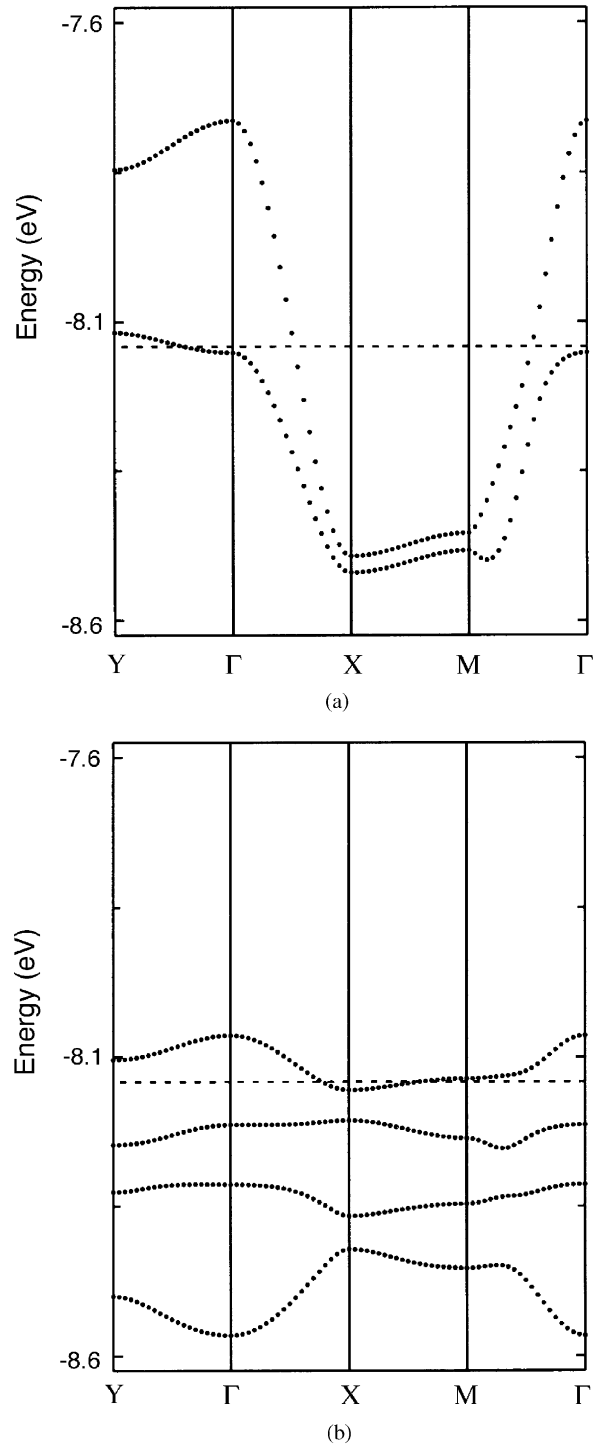

FIG. 10. (a) Dispersion relations of the two HOMO bands calculated for the donor Layer 1 of $(ET)_2C(SO_2CF_3)_3$. (b) Dispersion relations of the four HOMO bands calculated for the donor Layer 2 of $(ET)_2C(SO_2CF_3)_3$. The dashed line refers to the Fermi level.

the crystal structure prevents us from discussing further on the differences in the ET molecules. The nearly half-filled band of Layer 1 has a one-dimensional (1D) metallic

behavior along the *a*-axis (i.e., the interstack) direction (Fig. 10a), so that Layer 1 should be susceptible toward a charge density wave (CDW) formation associated with a pairing distortion along the *a*-axis direction. In contrast, the four bands of Layer 2 show weak dispersions (Fig. 10b), so that electrons at the bottom of the top band around X cannot induce metallic properties. The semiconducting behavior of $(ET)_2C(SO_2CF_3)_3$ below ~ 240 K implies that even around room temperature, Layer 1 should be unstable toward a CDW formation associated with a pairing distortion along the *a*-axis direction. The high spin susceptibility around room temperature might be due to a CDW fluctuation (45), i.e., a dynamic formation and destruction of CDW segments in donor Layer 1 without any long-range order between them. The MI transition of $(ET)_2C(SO_2CF_3)_3$ at ~ 180 K suggests that a CDW of long range order sets in below ~ 180 K (Fig. 6c). The sharp increase in spin susceptibility below ~ 50 K might be due to the occurrence of kinks (or domain walls) in the CDW formation, i.e., isolated patches of donor molecules in between ordered CDW regions. In the donor molecules located at such kinks, electrons can be localized hence leading to an enhancement of spin susceptibility.

To gain some insight into the origin of the MI transition in $(ET)_2CH(SO_2CF_3)_2$ at ~ 110 K, we examine how strongly nearest-neighbor ET molecules interact in donor Layers 1 and 2 by calculating the HOMO–HOMO interaction energy $\beta_{ij} = \langle \psi_i | H^{\text{eff}} | \psi_j \rangle$ (46), where H_{eff} is an effective Hamiltonian, and ψ_i and ψ_j are the HOMO's of ET molecules *i* and *j*, respectively. The β_{ij} values calculated for $(ET)_2CH(SO_2CF_3)_2$ are summarized in Table 2, which reveals that the intrastack interactions are much stronger than the interstack interactions, and that each donor stack is slightly dimerized. Our discussion in the previous section suggested that the MI transition of $(ET)_2CH(SO_2CF_3)_2$ at ~ 110 K is probably caused by a geometrical change that produces a normal semiconductor. A probable geometry change is one that reduces the interstack interactions. Such a change will make the resulting Fermi surface 1D and hence induce a dimerization in each donor stack, which leads to ET tetramers in each donor stack. It would be interesting to examine the crystal structure of $(ET)_2CH(SO_2CF_3)_2$ at a temperature below ~ 110 K.

TABLE 2
HOMO–HOMO Interaction Energies β_{ij} (in meV) between the Nearest-Neighbor ET Molecules in the Donor Molecule Layers of $(ET)_2CH(SO_2CF_3)_2$[a]

Layer	Intrastack	Interstack
Layer 1	$a = 452$	$c = 8$
	$a' = 357$	$d = 122$
		$d' = 61$
Layer 2	$a = 442$	$c = 48$
	$a' = 354$	$d = 82$
		$d' = 36$

[a] The intermolecular interactions are defined in Figs. 4b and 4c.

6. CONCLUDING REMARKS

Three 2:1 ET salts, $(ET)_2N(SO_2CF_3)_2$, $(ET)_2CH(SO_2CF_3)_2$ and $(ET)_2C(SO_2CF_3)_3$, were obtained by electrocrystallization with the anions $N(SO_2CF_3)_2^-$, $CH(SO_2CF_3)_2^-$, $C(SO_2CF_3)_3^-$. These salts differ in their donor molecule packing motifs and in their transport properties. $(ET)_2N(SO_2CF_3)_2$ is a 2D metal, but its ESR spin susceptibility above ~ 150 K shows a weakly semiconducting behavior. This discrepancy is due probably to the facts that the anions of this salt are disordered, and that during the ESR measurements the sample cooling rate is slow enough to allow the anions to readjust their positions at a given temperature. $(ET)_2CH(SO_2CF_3)_2$ is a 2D metal, and its MI transition at ~ 110 K is presumably due to a geometry change of the donor layers that reduces the interstack interactions. $(ET)_2C(SO_2CF_3)_3$ has a nearly half-filled 1D band, and its ESR spin susceptibility and electrical resistivity data suggest that it undergoes a CDW transition at around ~ 180 K.

Supplemental information available: Crystallographic data (excluding structure factors) for the structures reported in this paper have been deposited with the Cambridge Crystallographic Data Centre as supplementary publication no. CCDC 1928–192883. Copies of the data can be obtained free of charge on application to CCDC, 12 Union Road, Cambridge CB2 1EZ, UK (fax: (44) 1223 336-033; e-mail: deposit@ccdc.cam.ac.uk).

ACKNOWLEDGMENTS

Work at Argonne National Laboratory is sponsored by the US Department of Energy, Office of Basic Energy Sciences, Division of Materials Sciences, under Contract W-31-139-ENG-38. Research at Portland State University was supported by the National Science Foundation (CHE-9904316) and the Petroleum Research Fund (ACS-PRF 34624-AC7). Work at the North Carolina State University was supported by the US Department of Energy, Office of Basic Sciences, Division of Materials Sciences, under Grant DE-FG02-86ER45259.

REFERENCES

1. J. M. Williams, J. R. Ferraro, R. J. Thorn, K. D. Carlson, U. Geiser, H. H. Wang, A. M. Kini, and M. H. Whangbo, Organic Superconductors (Including Fullerenes). Prentice–Hall, Englewood Cliffs, NJ, 1992.
2. T. Ishiguro, K. Yamaji, and G. Saito, Organic Superconductors. Springer-Verlag, Berlin, Heidelberg, New York, 1998.

3. W. A. Little, *in* "Organic Conductors" (J.-P. Farges Ed.), pp. 1–24. Marcel Dekker, Inc., New York, 1994.
4. M. Lang, *Supercond. Rev.* **2,** 1–115 (1996).
5. J. M. Williams, A. M. Kini, H. H. Wang, K. D. Carlson, U. Geiser, L. K. Montgomery, G. J. Pyrka, D. M. Watkins, J. M. Kommers, S. J. Boryschuk, A. V. Strieby Crouch, W. K. Kwok, J. E. Schirber, D. L. Overmyer, D. Jung, and M.-H. Whangbo, *Inorg. Chem.* **29,** 3272–3274 (1990).
6. J. A. Schlueter, U. Geiser, A. M. Kini, H. H. Wang, J. M. Williams, D. Naumann, T. Roy, B. Hoge, and R. Eujen, *Coord. Chem. Rev.* **190–192,** 781–810 (1999).
7. J. A. Schlueter, U. Geiser, J. M. Williams, H. H. Wang, W. K. Kwok, J. A. Fendrich, K. D. Carlson, C. A. Achenbach, J. D. Dudek, D. Naumann, T. Roy, J. E. Schirber, and W. R. Bayless, *J. Chem. Soc. Chem. Commun.* 1599–1600 (1994).
8. J. A. Schlueter, K. D. Carlson, U. Geiser, H. H. Wang, J. M. Williams, W. K. Kwok, J. A. Fendrich, U. Welp, P. M. Keane, J. D. Dudek, A. S. Komosa, D. Naumann, T. Roy, J. E. Schirber, W. R. Bayless, and B. Dodrill, *Physica C* **233,** 379–386 (1994).
9. J. A. Schlueter, J. M. Williams, U. Geiser, J. D. Dudek, S. A. Sirchio, M. E. Kelly, J. S. Gregar, W. H. Kwok, J. A. Fendrich, J. E. Schirber, W. R. Bayless, D. Naumann, and T. Roy, *J. Chem. Soc. Chem. Commun.* 1311–1312 (1995).
10. J. A. Schlueter, J. M. Williams, U. Geiser, J. D. Dudek, M. E. Kelly, S. A. Sirchio, K. D. Carlson, D. Naumann, T. Roy, and C. F. Campana, *Adv. Mater.* **7,** 634–639 (1995).
11. J. A. Schlueter, U. Geiser, H. H. Wang, M. E. Kelly, J. D. Dudek, J. M. Williams, D. Naumann, and T. Roy, *Mol. Cryst. Liq. Cryst.* **284,** 195–202 (1996).
12. U. Geiser, J. A. Schlueter, J. D. Dudek, J. M. Williams, D. Naumann, and T. Roy, *Acta Crystallogr. C* **51,** 1779–1782 (1995).
13. U. Geiser, J. A. Schlueter, H. H. Wang, A. M. Kini, J. M. Williams, P. P. Sche, H. I. Zakowicz, M. L. VanZile, J. D. Dudek, P. G. Nixon, R. W. Winter, G. L. Gard, J. Ren, and M.-H. Whangbo, *J. Am. Chem. Soc.* **118,** 9996–9997 (1996).
14. A. Webber, *J. Electrochem. Soc.* **138,** 2586–2590 (1991).
15. N. R. Holcomb, P. G. Nixon, G. L. Gard, R. L. Nafshun, and M. M. Lerner, *J. Electrochem. Soc.* **143,** 1297–1300 (1996).
16. H. H. Wang, U. Geiser, M. E. Kelly, M. L. Vanzile, A. J. Skulan, J. M. Williams, J. A. Schlueter, A. M. Kini, S. A. Sirchio, and L. K. Montgomery, *Mol. Cryst. Liq. Cryst.* **284,** 427–436 (1996).
17. T. K. Hansen, J. Becher, T. Jorgensen, K. S. Varma, R. Khedekar, and M. P. Cava, *Org. Synth.* **73,** 270–277 (1995).
18. K. S. Varma, A. Bury, N. J. Harris, and A. E. Underhill, *Synthesis* 837–838 (1987).
19. T. J. Emge, H. H. Wang, M. A. Beno, J. M. Williams, M. H. Whangbo, and M. Evain, *J. Am. Chem. Soc.* **108,** 8215–8223 (1986).
20. D. A. Stephens, A. E. Rehan, S. J. Compton, R. A. Barkhau, and J. M. Williams, *Inorg. Synth.* **24,** 135–137 (1986).
21. J. A. Schlueter, A. M. Kini, U. Geiser, H. H. Wang, unpublished work.
22. T. Mori, *Bull. Chem. Soc. Jpn.* **71,** 2509–2526 (1998).
23. B. H. Ward, J. A. Schlueter, U. Geiser, H. H. Wang, E. Morales, J. Parakka, S. Y. Thomas, J. M. Williams, P. G. Nixon, R. W. Winter, G. L. Gard, H. J. Koo, and M. H. Whangbo, *Chem. Mater.* **12,** 343–351 (2000).
24. P. Guionneau, C. J. Kepert, G. Bravic, D. Chasseau, M. R. Truter, M. Kurmoo, and P. Day, *Synth. Met.* **86,** 1973–1974 (1997).
25. Z. Zak, A. Ruzicka, and C. Michot, *Z. Kristallogr.* **213,** 217–222 (1998).
26. J. L. Nowinski, P. Lightfoot, and P. G. Bruce, *J. Mater. Chem.* **4,** 1579–1580 (1994).
27. A. Haas, C. Klare, P. Betz, J. Bruckmann, C. Krüger, Y. H. Tsay, and F. Aubke, *Inorg. Chem.* **35,** 1918–1925 (1996).
28. J. J. Golding, D. R. MacFarlane, L. Spiccia, M. Forsyth, B. W. Skelton, and A. H. White, *J. Chem. Soc. Chem. Commun.* 1593–1594 (1998).
29. S. Z. Zhu, *J. Fluorine Chem.* **62,** 31–37 (1993).
30. A. R. Siedle, W. B. Gleason, R. A. Newmark, and L. H. Pignolet, *Organometallics* **5,** 1969–1975 (1986).
31. K. T. Davoy, T. Gramstad, and S. Husebye, *Acta Chem. Scand. A* **33,** 359–363 (1979).
32. A. R. Siedle, R. A. Newmark, and L. H. Pignolet, *Inorg. Chem.* **1986,** 3412–3418 (1986).
33. T. Mori, H. Mori, and S. Tanaka, *Bull. Chem. Soc. Jpn.* **72,** 179–197 (1999).
34. L. Turowsky and K. Seppelt, *Inorg. Chem.* **27,** 2135–2137 (1988).
35. H. H. Wang, M. L. VanZile, J. A. Schlueter, U. Geiser, A. M. Kini, P. P. Sche, H. J. Koo, M. H. Whangbo, P. G. Nixon, R. W. Winter, and G. L. Gard, *J. Phys. Chem. B* **103,** 5493–5499 (1999).
36. N. F. Mott, "Metal–Insulator Transitions". Barnes and Noble, New York, 1977.
37. B. H. Brandow, *Adv. Phys.* **26,** 651–808 (1977).
38. M. H. Whangbo, *J. Chem. Phys.* **70,** 4963–4966 (1979).
39. H. H. Whangbo, and R. Hoffmann, *J. Am. Chem. Soc.* **100,** 6093–6098 (1978).
40. J. Ren, W. Liang, and M. H. Whangbo, "Crystal and Electronic Structure Analysis Using *CAESAR*." PrimeColor Software, Inc., 1998 (http://www.PrimeC.com/).
41. M.-H. Whangbo, J. M. Williams, P. C. W. Leung, M. A. Beno, T. J. Emge, H. H. Wang, K. D. Carlson, and G. W. Crabtree, *J. Am. Chem. Soc.* **107,** 5815–5816 (1985).
42. J. S. Brooks, G. J. Athas, S. J. Klepper, X. Chen, C. E. Campana, S. Valfells, Y. Tanaka, T. Kinoshita, M. Tokumoto, and H. Anzai, *Physica B* **201,** (1994) 449–458, and the references cited therein.
43. T. Sasaki, H. Sato, and N. Toyota, *Solid State Commun.* **76,** 507–510 (1990).
44. H. Müller, C.-P. Heidmann, A. Lerf, W. Biberacher, R. Sieburger, and K. Andres, *in*: "The Physics and Chemistry of Organic Superconductors" (G. Saito, S. Kagoshima Eds), pp. 195–199. Springer-Verlag, Berlin, Heidelberg, 1990.
45. R. Moret, J. P. Pouget, *in* "Crystal Chemistry and Properties of Materials with Quasi-One-Dimensional Structures" (J. Rouxel Ed.), p. 87. Reidel, Dordrecht, The Netherlands, 1986.
46. M.-H. Whangbo, J. M. Williams, P. C. W. Leung, M. A. Beno, T. J. Emge, and H. H. Wang, *Inorg. Chem.* **24,** 3500–3501 (1985).